The British Journal of Radiology, 80 (2007), 911–918

Analysis of streak artefacts on CT images using statistics of extremes

[1]K IMAI, PhD, [1]M IKEDA, MD, [2]S WADA, PhD, [3]Y ENCHI, MSc and [1]T NIIMI, BSc

[1]*Department of Radiological Technology, Nagoya University School of Health Sciences, 1-20 Daikominami 1-chome, Higashi-ku, Nagoya 461-8673,* [2]*Division of Radiological Technology, Niigata University School of Health Sciences, 746 Asahimachi-dori 2-bancho, Niigata 951-8518 and* [3]*Division of Radiological Technology, Osaka University Hospital, 2-15 Yamadaoka, Suita, Osaka 565-0971, Japan*

ABSTRACT. We have analysed the statistical characteristics of streak artefacts on CT images using the statistics of extremes, and have devised a new method of evaluating streak artefacts on CT images. The CT images of four polymer tubes placed on the chest wall of a commercially available chest phantom were used as the target objects for our analysis. 40 parallel line segments with a length of 20 pixels were placed perpendicular to numerous streak artefacts on the polymer tube image, and the largest difference between adjacent CT values in each of the 40 CT value profiles of these line-segments was employed as a feature variable of a streak artefact; these feature variables have been analysed by extreme value theory. Using the mean rank method, a Gumbel distribution was shown to be the most suitable extreme value distribution for the largest difference between adjacent CT values in each CT value profile. This enabled us to demonstrate that the streak artefacts on CT images can be statistically modelled by a Gumbel distribution. Both the location parameter and the scale parameter of the estimated Gumbel probability density distribution were large on the CT slices in which the shoulder bone or liver was included.

Received 21 September 2006
Revised 12 March 2007
Accepted 27 March 2007

DOI: 10.1259/bjr/93741044

In the past few decades, CT scanners have made remarkable progress, thanks to the development of image processing technology and the introduction of a helical scanning algorithm. These improvements have made it possible to depict tiny and subtle lesions, such as small pulmonary nodules. Furthermore, helical CT reduces scan times, enabling an entire scan of the chest and abdomen to be performed in a single held breath. In the near future, by superseding conventional radiography systems, CT will play a central role as a clinical screening tool (e.g. in lung cancer screening).

However, the radiation doses of CT examinations are relatively high compared with those of the other radiological modalities. More recently, many studies have been conducted on low-dose CT screening with a multidetector row helical CT (MDCT) scanner [1–5]. The potential disadvantage of performing low-dose CT examinations is the degradation of image quality as the radiation dose is reduced. In particular, the streak artefacts that are problematic for image diagnosis increase noticeably in low-dose CT images [6, 7]. Although the exact mechanism of these streak artefacts remains obscure, it is safe to say that they are caused by X-ray photon starvation; in other words, when an X-ray beam passes through highly attenuated areas such as shoulders, noisy projections will be produced in the attenuation direction and the reconstruction process will have the effect of greatly magnifying the noise, resulting in streak artefacts on the CT image [8, 9]. Thus, it is important to evaluate such artefacts in relation to a given radiation dose.

At the present time, there are several methods for quantifying the spatial resolution and image noise of CT images; for example, the former is evaluated by a modulation transfer function [10, 11] and a full-width at half maximum value of a δ functional image [12, 13], whereas the latter is assessed quantitatively by a standard deviation (SD) of pixel values in a region of interest placed in a homogeneous background [14, 15].

However, as there is no definitive quantitative descriptor of artefacts on CT images, each one has to be assessed by a human observer based on a rating method [6, 16–19]. In order to obtain an accurate result using this method, many observers must participate in image-reading experiments, which are time-consuming and tedious. Therefore, if an objective and quantitative method of evaluating artefacts on CT images is developed, it will surely prove very useful.

As a result, we have analysed the statistical characteristics of streak artefacts on CT images using the statistics of extremes [20], and have devised a new method of evaluating them.

Methods and materials

CT image acquisition

In this study, a commercially available chest phantom (CT Torso Phantom, CTU-Type 4; Kyoto-Kagaku Co.

Address correspondence to: Kuniharu Imai, Assistant Professor, Department of Radiological Technology, Nagoya University School of Health Sciences, 1-20 Daikominami 1-chome, Higashi-ku, Nagoya 461-8673, Japan. E-mail: imai@met.nagoya-u.ac.jp

This study was supported by a Grant-in-Aid for Scientific Research on Priority Areas 15070205 from the Ministry of Education, Culture, Sports, Science and Technology of Japan.

Ltd, Kyoto, Japan) was used. To evaluate streak artefacts and noises against homogeneous backgrounds, four polymer tubes filled with water were placed on the chest wall of the phantom; the direction of the long axis of the tubes was set parallel to the sagittal direction of the chest phantom. The space between polymer tubes I and II was 50 mm, between III and IV it was 50 mm, and between II and III it was 70 mm. Each tube was made of polyethylene with a diameter of 30 mm. The entire chest phantom was scanned using a 16-multidetector-row helical CT scanner (Aquilion; Toshiba Co. Ltd, Tokyo, Japan) with a collimation of 1 mm, a pitch of 1.5, a 0.5 s gantry rotation period, a tube voltage of 120 kVp, and a tube current of 10 mA (low enough to generate streak artefacts on CT image for all slices). Under routine conditions, tube current was 300 mA. All CT images were reconstructed with three different reconstruction kernels: FC01 (for soft-tissue imaging), FC50 (for lung imaging), and FC52 (for high-contrast lung imaging). The images were transferred from the CT scanner to a

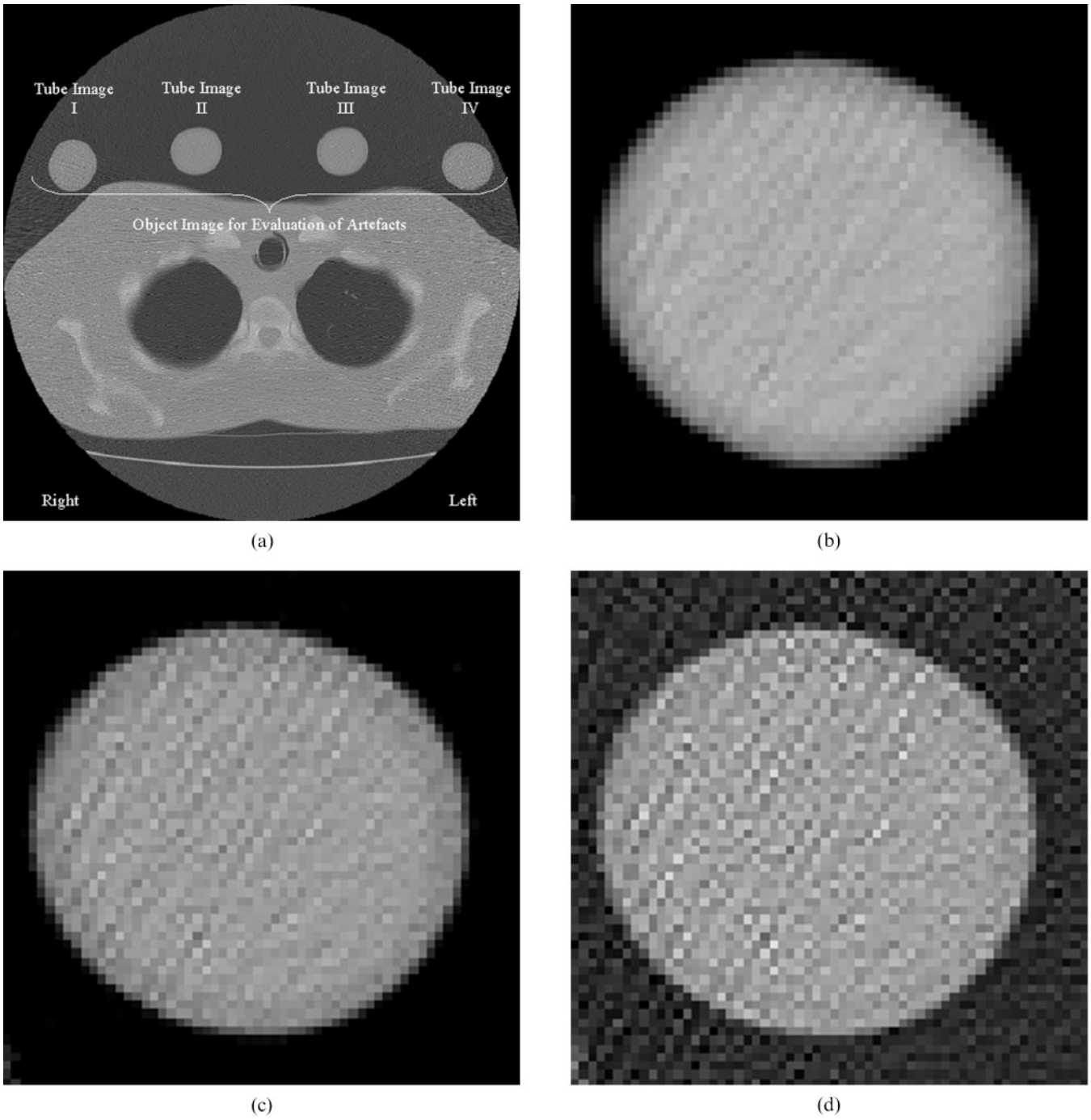

Figure 1. (a) CT image of the upper zone of a chest phantom and four polymer tubes filled with water placed on the chest wall. The images of polymer tubes I, II, III and IV were used as target objects to evaluate streak artefacts. (b) Magnified image of polymer tube I, which was reconstructed by the FC01 reconstruction kernel. (c) Magnified image of polymer tube I, which was reconstructed by the FC50 reconstruction kernel. (d) Magnified image of polymer tube I, as reconstructed by the FC52 reconstruction kernel. Streak artefacts increased in order of FC01<FC50<FC52.

personal computer using the standard file format with a matrix size of 512×512 and a grey level of 16 bits according to Digital Imaging and Communications in Medicine (DICOM) format. Figure 1 shows sample polymer tube images.

Extreme value theory

The CT images of the four polymer tubes placed on the chest wall of the phantom were used as target objects for our analysis of the streak artefacts. We measured 40 parallel line profiles of CT numbers — each 20 pixels in length — in the central portion of each polymer tube image, and placed them almost perpendicular to numerous streak artefacts. Here, the streak artefacts on the polymer tube images were visually recognized on the CT images through a display window with a width of 2500 Hounsfield units (HU) and a level of –600 HU (these display window conditions correspond to those for evaluating lung fields). The directions of the streak artefacts were manually determined by one of the authors. The CT values fluctuate greatly around the streak artefacts and it is impossible to identify the exact positions of the artefacts on each CT value profile, as value variations caused by the artefacts cannot be distinguished from other unspecified image noise. Thus, it is very difficult to analyse the artefacts by conventional statistical parameters, such as the mean and SD of CT values.

From these CT value profile curves, the largest difference between adjacent CT values was estimated empirically to be attributable to streak artefacts, and that became our focus. Furthermore, the 40 largest differences between adjacent CT values can be considered as the largest among an extensive set of independent and identically distributed random values, and can be modelled by a generalized extreme value distribution [20]. Here, we confirmed that the largest values did not seriously violate the assumption of independence by drawing their scatter plots. We therefore consider the largest difference between adjacent CT values in each CT value profile as a feature variable of the streak artefacts, and have analysed them using the statistics of extremes [20].

The statistics of extremes states that the probability distribution of the largest values among a large set of independent and identically distributed random values will asymptotically converge to one of the generalized extreme value distributions. That is, the maximum of a sequence of observations will be approximately distributed as a generalized extreme value distribution, which can be further categorized into the following three distributions: Gumbel distribution (Extreme Value Type I), Frechet distribution (Extreme Value Type II), and Weibull distribution (Extreme Value Type III) [20]. These are the limit distributions, regardless of the underlying distributions such as the normal distribution; in this study, the distribution of CT value variations caused by both streak artefacts and other unspecified image noises was considered to be the underlying distribution. The three classes of limit distributions for extreme values exhibit different behaviour in the extreme tail of the underlying distribution. Those distributions whose tails decrease exponentially, such as the exponential distribution, lead to the Gumbel distribution (Equation 1); those whose tails decrease as a polynomial, such as Student's t distribution, lead to the Frechet distribution (Equation 2); and those with finite tails, such as the β distribution, lead to the Weibull distribution (Equation 3) [20]. These distributions are expressed as follows:

$$F(x) = \exp\left[-\exp\left(-\frac{x-\beta}{\gamma}\right)\right] \quad (1)$$

$$F(x) = \exp\left[-\left(\frac{x-\beta}{\gamma}\right)^{-\alpha}\right] \quad (2)$$

Table 1. Relationship between the largest difference between adjacent CT values in each CT value profile and the cumulative probability estimated by the mean rank method ($n=40$).

Order	Estimated cumulative probability	Largest difference	Order	Estimated cumulative probability	Largest difference
1	0.0244	143	21	0.5122	218
2	0.0488	151	22	0.5366	218
3	0.0732	155	23	0.5610	221
4	0.0976	164	24	0.5854	224
5	0.1220	167	25	0.6100	235
6	0.1463	168	26	0.6341	236
7	0.1707	176	27	0.6585	238
8	0.1951	184	28	0.6829	239
9	0.2195	184	29	0.7073	244
10	0.2439	185	30	0.7317	245
11	0.2683	186	31	0.7561	256
12	0.2927	187	32	0.7805	263
13	0.3171	187	33	0.8049	275
14	0.3415	187	34	0.8293	278
15	0.3659	188	35	0.8537	286
16	0.3902	197	36	0.8780	301
17	0.4146	204	37	0.9024	303
18	0.4390	206	38	0.9268	308
19	0.4634	212	39	0.9512	363
20	0.4878	214	40	0.9756	382

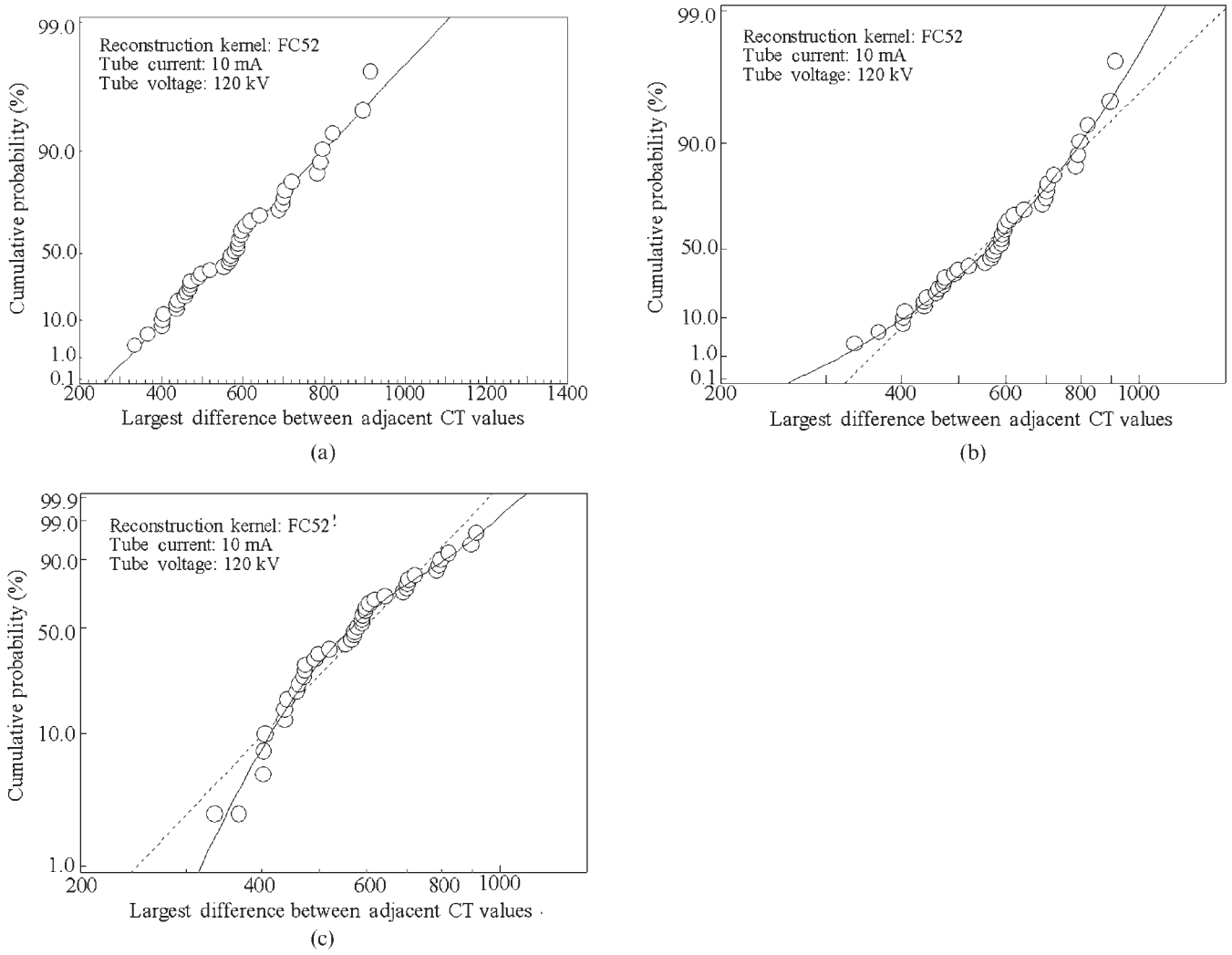

Figure 2. Plot of estimated cumulative probability function versus the largest difference between adjacent CT values for data given in Table 1. (a) Gumbel plot. Straight line represents line fitted to data (r=0.992). (b) Frechet plot. Curved line represents quadratic polynomial fitted to data (r=0.992). Broken straight line represents linear polynomial fitted to data (r=0.975). (c) Weibull plot. Curved line represents quadratic polynomial fitted to data (r=0.991). Broken straight line represents linear polynomial fitted to data (r=0.966).

$$F(x)=\exp\left[-\left(\frac{\beta-x}{\gamma}\right)^{\alpha}\right] \quad (3)$$

where $F(x)$ is the cumulative probability function for the maximum random variable x, and α, β and γ are shape, location and scale parameters, respectively. The shape parameter corresponds to the shape of the probability density distribution; the location parameter to the mode of that distribution; and the scale parameter to its variance.

Estimation of distribution of extreme values

The unknown cumulative probability function $F(x)$ can be estimated using the mean rank method with ''order statistics''. We employed this estimation method because it will achieve high accuracy in calculating cumulative probabilities, and its use was recommended by Gumbel [20]. Thus, for the largest difference between adjacent CT values in each CT value profile, x, the estimated cumulative probability function $\hat{F}(x)$ was derived as follows.

The 40 largest differences between adjacent CT values on each polymer tube image were arranged in ascending order: $x_{(1)} \le x_{(2)} \le \ldots \le x_{(40)}$. Then, $\hat{F}(x_{(i)})$ was computed as:

$$\hat{F}(x_{(i)})=\frac{i}{n+1}, \quad \text{for } i=1,\ldots,n \quad (4)$$

where n is a sampling size (in this study, n=40). To determine which of the three types of generalized extreme value distribution is the most appropriate model for the data considered in this study, we plotted the estimated cumulative probability function against the largest difference between adjacent CT values following the Gumbel, Frechet and Weibull plots, respectively. If the estimated cumulative probability function is reasonably representative of the generalized extreme value distribution, those plots will be linear.

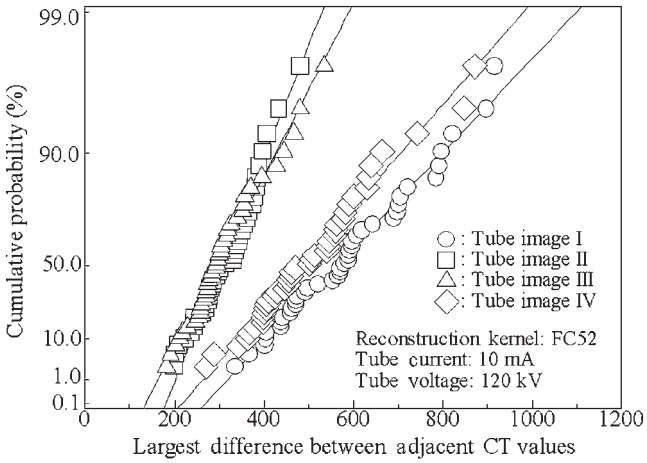

Figure 3. Gumbel plot of estimated cumulative probability function versus largest difference between adjacent CT values for data on images of polymer tubes I, II, III and IV shown in Figure 1a. Images were reconstructed using the FC52 reconstruction kernel.

When the fitting line for the Gumbel plot is expressed as $ax+b$, the scale parameter γ and the location parameter β are given by $\gamma=1/a$ and $\beta=\gamma b$, because

$$-\ln\{-\ln[F(x)]\}=\frac{1}{\gamma}x-\frac{\beta}{\gamma} \qquad (5)$$

In this study, we estimated the Gumbel distribution from the parameters a and b, obtained by line-fitting on the Gumbel plot. Furthermore, we propose to employ the location and the scale parameters of the Gumbel probability density distribution as the feature indices in the Gumbel evaluation method. As stated above, those indices can be estimated from the parameters a and b.

Results

The relationship between the largest difference between adjacent CT values and its estimated cumulative probability in Figure 1c is shown in Table 1, whereas Figure 2a–c shows the Gumbel, Frechet and Weibull plots for this relationship, respectively. In the Gumbel plot, the largest differences between adjacent CT values were distributed linearly. Conversely, the Frechet and Weibull plots showed a slight departure from linearity, making a Gumbel distribution the most suitable for the largest difference between adjacent CT values in each CT value profile. Similar results were also obtained for other data on the polymer tube images. Therefore, for a statistical model of the largest difference between adjacent CT values in each CT value profile, we adopt a Gumbel distribution, and propose to evaluate the streak artefacts on CT images using the largest difference between adjacent CT values and its Gumbel distribution. Hereafter, we refer to this as the ''Gumbel evaluation method''.

Figure 3 shows the Gumbel plot of the estimated cumulative probability function versus the largest difference between adjacent CT values on each polymer tube image shown in Figure 1a. The gradients of the fitted lines for their Gumbel plots of the images of polymer tubes I and IV were smaller than those of the images of polymer tubes II and III.

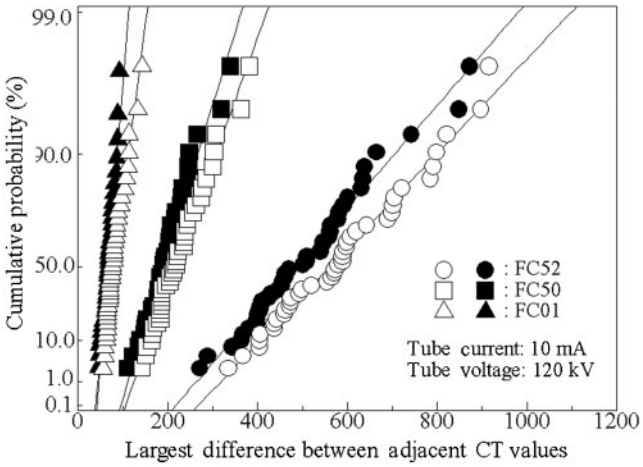

Figure 4. Gumbel plots of estimated cumulative probability function versus largest difference between adjacent CT values for data on images of polymer tubes I and IV in Figure 1a, as reconstructed by reconstruction kernels FC01, FC50 and FC52. White circles represent data on polymer tube I, reconstructed by the FC52 reconstruction kernel; black circles on polymer tube IV reconstructed by FC52; white squares on polymer tube I reconstructed by FC50; black squares on polymer tube IV reconstructed by FC50; white triangles on polymer tube I reconstructed by FC01; and black triangles on polymer tube IV reconstructed by FC01.

The relationship between the streak artefacts and the reconstruction algorithms was investigated quantitatively by the Gumbel evaluation method for the images of polymer tubes I and IV in Figure 1a. It was shown that the streak artefacts on the images of the polymer tubes in the CT slice of the upper zone of the chest phantom varied dramatically, depending on the reconstruction algorithms (Figure 4). Furthermore, the Gumbel probability density distribution indicated this even more clearly (Figure 5).

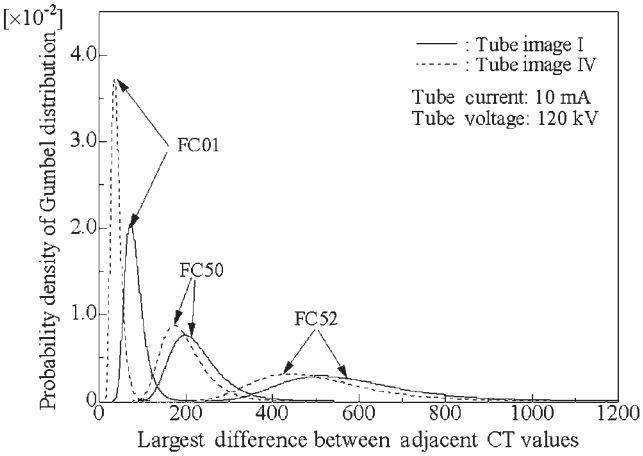

Figure 5. Gumbel probability density distributions estimated from Gumbel plots shown in Figure 4. These distributions are for data on polymer tube I and IV images, as reconstructed by kernels FC01, FC50 and FC52. The solid line represents the Gumbel probability density distribution obtained from data on the polymer tube I image, and the broken line from data on the polymer tube IV image.

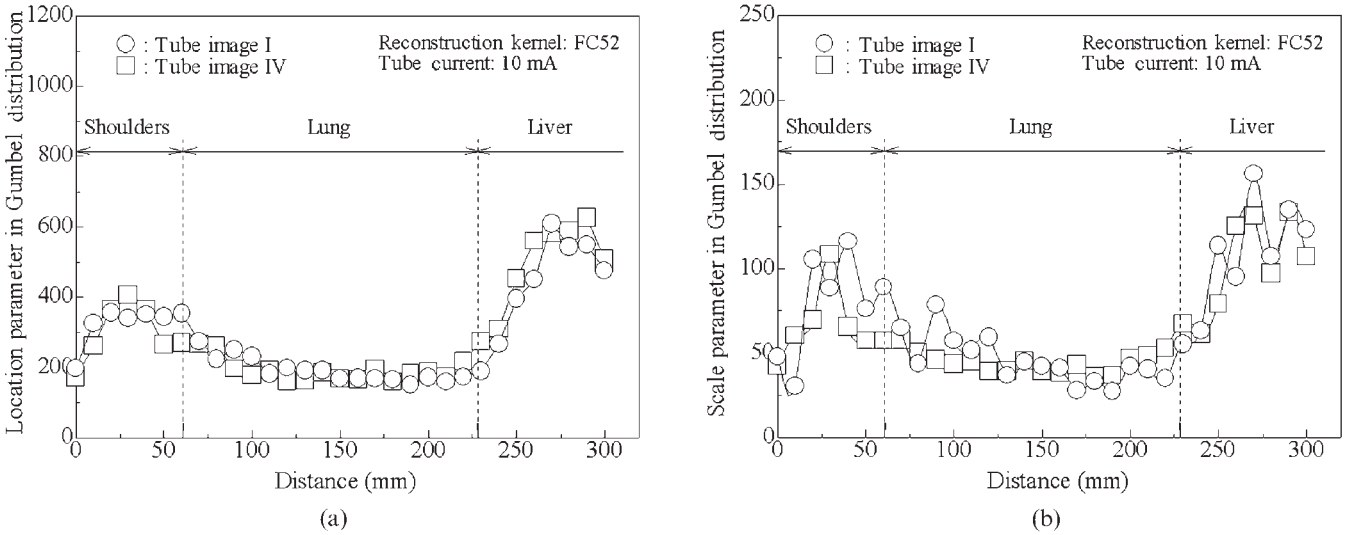

Figure 6. (a) Relationship of the location parameter of the Gumbel probability density distribution estimated for the largest difference between adjacent CT values in each CT value profile and CT slice position. (b) Relationship between the scale parameter of the Gumbel distribution and CT slice position. Here, distance is from the top of the lung field in the chest phantom.

The streak artefacts and their variations on the images of the polymer tubes reconstructed by the FC01 kernel were small compared with the other kernels, whereas the streak artefacts by the FC52 kernel and their variations were large.

Figure 6 shows the result of evaluating the streak artefacts on the polymer tube images in each CT slice by the feature indices using the Gumbel evaluation method. Both the location parameter and the scale parameter of the Gumbel probability density distribution estimated for the largest difference between adjacent CT values in each CT value profile were larger on CT slices in which the shoulder, bone or liver was included than on other slices. These results were consistent with the subjective recognition of the streak artefacts on the CT images with a display window width of 2500 HU and a level of −600 HU (Figure 7).

Discussion

We have shown that the largest difference between adjacent CT values in each CT value profile on the polymer tube image can be statistically modeled by a Gumbel distribution and, based on this result, we have devised a new method of evaluating the streak artefacts on CT images that we call the ''Gumbel evaluation method''. Using that method, the streak artefacts on the polymer tube image on CT slices in which the shoulder bone or liver was included were shown to be larger than those from other slices. Several studies have shown that streak artefacts often occur on the CT images, causing a major difference in attenuation with the rotational position of the X-ray tube [8, 9]. In this study, such situations correspond to the tube images near the shoulder or the liver, thus demonstrating that the results of analysing streak artefacts by our new method are reasonable.

The statistical analysis was performed for the largest difference between adjacent values in each CT value profile. These data can be considered equivalent to the image data processed by a one-dimensional difference operator [21]. Therefore, neglecting the residual component of the noise-free image, these data would be equivalent to the noise component of the original CT image [21], and their values would be expected to be large at the positions of streak artefacts.

Streak artefacts have an undeniably detrimental effect on the diagnostic performance of radiologists and computer-aided diagnostic systems. Additionally, such artefacts on CT images are empirically known to increase as the radiation dose decreases [6, 7]. Thus, the evaluation of streak artefacts is important in solving the problem of estimating lower limits for dose while maintaining satisfactory diagnostic performance. Although the streak artefacts on CT images can be considered to follow some underlying rules, they are still unknown as an analytic form as far as we know. Thus, the Gumbel evaluation method is expected to prove useful in determining the most appropriate reduction in the radiation dosage.

Our method gives a local assessment of the level of streak artefacts at a given location and in a selected direction, *i.e.* it is a direction-dependent method. However, an ideal method for evaluating streak artefacts should be independent of direction. This problem deserves further consideration.

More recently, many studies have been conducted on CT screening using an MDCT scanner with automatic tube-current modulation [22, 23]. This technique enables automatic adjustment of the tube current according to the size and attenuation characteristics of the body part being scanned, increasing the tube current for the highest attenuation projection direction and reducing it for a low attenuation direction. One of the aims of this technique is to reduce streak artefacts. However, the reductions seen in streak artefacts have not been clarified. Therefore, the Gumbel evaluation method can be used to quantitatively assess how well this system works.

Conclusions

We have demonstrated that the largest difference between adjacent CT values in each CT value profile on a polymer tube image can be statistically modelled by a

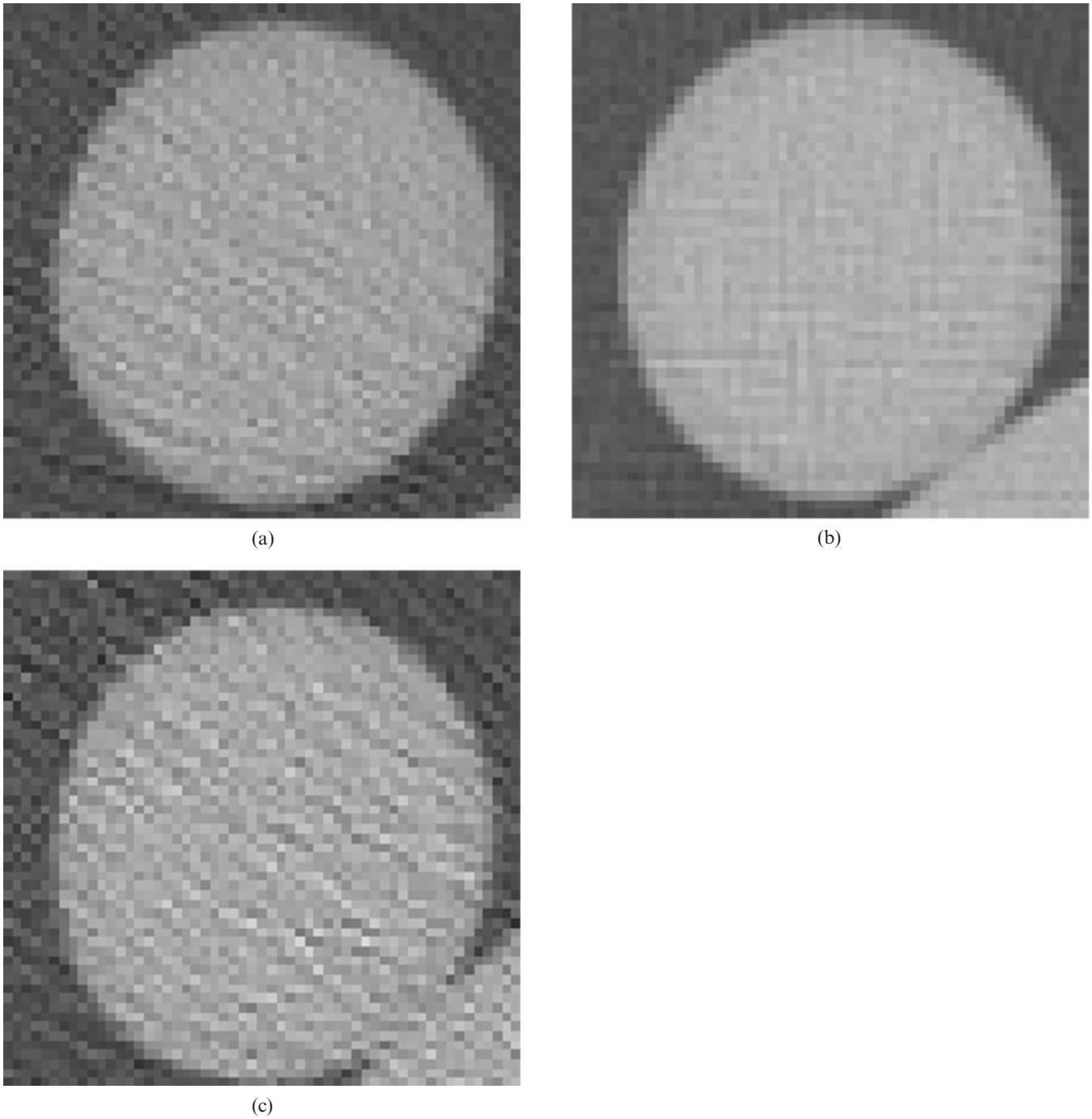

Figure 7. (a) Magnified image of polymer tube I at a distance of 40 mm in Figure 6; the polymer tube was in the shoulder bone area. (b) Magnified image of polymer tube I at a distance of 150 mm in Figure 6; the polymer tube was in the lung area. (c) Magnified image of polymer tube I at a distance of 280 mm in Figure 6. The streak artefacts increased in the order of (b)<(a)<(c).

Gumbel distribution and, based on that result, we have devised a new method of evaluating streak artefacts on CT images that we call the ''Gumbel evaluation method''.

Acknowledgment

This study was supported by a Grant-in-Aid for Scientific Research on Priority Areas 15070205 from the Ministry of Education, Culture, Sports, Science and Technology of Japan.

References

1. Diederich S, Lenzen H, Windmann R, Puskas Z, Yelbuz TM, Henneken S, et al. Pulmonary nodules: experimental and clinical studies at low-dose CT. Radiology 1999;213:289–98.
2. Itoh S, Ikeda M, Mori Y, Suzuki K, Sawaki A, Iwano S, et al. Lung: feasibility of a method for changing tube current during low-dose helical CT. Radiology 2002;224:905–12.
3. Karabulut N, Törü M, Gelebek V, Gülsün M, Ariyurek OM. Comparison of low-dose and standard-dose helical CT in the evaluation of pulmonary nodules. Eur Radiol 2002;12: 2764–9.

4. Wormanns D, Ludwig K, Beyer F, Heindel W, Diederich S. Detection of pulmonary nodules at multirow-detector CT: effectiveness of double reading to improve sensitivity at standard-dose and low-dose chest CT. Eur Radiol 2005;15:14–22.
5. Gurung J, Khan MF, Maataoui A, Herzog C, Bux R, Bratzke H, et al. Multislice CT of the pelvis: dose reduction with regard to image quality using 16-row CT. Eur Radiol 2005;15:1898–905.
6. Lucaya J, Piqueras J, Garcia-Pena P, Enriquez G, Garcia-Macias M, Sotil J. Low-dose high-resolution CT of the chest in children and young adults: dose, cooperation, artifact incidence, and image quality. AJR Am J Roentgenol 2000;175:985–92.
7. Rusinek H, Naidich DP, McCuinness G, Leitman BS, McCaoley DI, Krinsky GA, et al. Pulmonary nodule detection: low-dose versus conventional CT. Radiology 1998;209:243–9.
8. Barrett FF, Keat N. Artifact in CT: recognition and avoidance. Radiographics 2004;24:1697–91.
9. Hsieh J. Adaptive streak artifact reduction in computed tomography resulting from excessive x-ray photon noise. Med Phys 1998;25:2139–47.
10. Kalra MK, Wittram C, Maher MM, Sharma A, Avinash GB, Karau K, et al. Can noise reduction filters improve low-radiation-dose chest CT images? Pilot study. Radiology 2003;228:257–64.
11. Boedeker KL, McNitt-Gray MF, Rogers SR, Truong DA, Brown MS, Gjertson DW, et al. Emphysema: effect of reconstruction algorithm on CT imaging measures. Radiology 2004;232:295–301.
12. Venema HW, Phoa SS, Mirck PG, Hulsmans FJ, Majoie CB, Verbeeten B, Jr. Petrosal bone: coronal reconstructions from axial spiral CT data obtained with 0.5-mm collimation can replace direct coronal sequential CT scans. Radiology 1999;213:375–82.
13. Brink JA, Heiken JP, Balfe DM, Sagel SS, DiCroce J, Vannier MW. Spiral CT: decreased spatial resolution in vivo due to broadening of section-sensitivity profile. Radiology 1992;185:469–74.
14. Greess H, Lutze J, Nömayr A, Wolf H, Hothorn T, Kalender WA, et al. Dose reduction in subsecond multislice spiral CT examination of children by online tube current modulation. Eur Radiol 2004;14:995–9.
15. Gündoğdu S, Mahmutyazicioğlu K, Özdemir H, Savranlar A, Asil K. Assessment of image quality of a standard and three dose-reducing protocols in adult cranial CT. Eur Radiol 2005;15:1959–68.
16. Boiselle PM, Hasegawa I, Nishino M, Raptopoulos V, Hatabu H. Comparison of artifacts on coronal reformation and axial CT pulmonary angiography images using single-detector and 4- and 8-detector multidetector-row helical CT scanners. Acad Radiol 2005;12:602–7.
17. Alberico RA, Loud P, Pollina J, Greco W, Patel M, Klufas R. Thick-section reformatting of thinly collimated helical CT for reduction of skull base-related artifacts. AJR Am J Roentgenol 2000;175:1361–6.
18. Wong K, Paulson EK, Nelson RC. Breath-hold three-dimensional CT of the liver with multi-detector row helical CT. Radiology 2001;219:75–9.
19. Montaudon M, Berger P, Blachère H, De Boucaud L, Latrabe V, Laurent F. Thin-section CT of the lung: influence of 0.5-s gantry rotation and ECG triggering on image quality. Eur Radiol 2001;11:1681–7.
20. Gumbel. Statistics of extremes. New York, USA: Columbia University Press; 1958.
21. Rank K, Lendl M, Unbehauen R. Estimation of image noise variance. IEE Proceedings — Vision, Image, and Signal Processing 1999;146:80–4.
22. Graser A, Wintersperger BJ, Suess C, Reiser MF, Becker CR. Dose reduction and image quality in MDCT colonography using tube current modulation. AJR Am J Roentgenol 2006;187:695–701.
23. Tack D, De Maertelaer V, Gevenois PA. Dose reduction in multidetector CT using attenuation-based online tube current modulation. AJR Am J Roentgenol 2003;187:695–701.